

Uncertainty analysis in the measurement of the spatial responsivity of infrared antennas

José Manuel López-Alonso, Brian Monacelli, Javier Alda, and Glenn Boreman

The measurement of a two-dimensional spatial responsivity map of infrared antennas can be accomplished by use of an iterative deconvolution algorithm. The inputs of this algorithm are the spatial distribution of the laser beam irradiance illuminating the antenna-coupled detector and a map of the measured detector response as it moves through the illuminating beam. The beam irradiance distribution is obtained from knife-edge measurements of the beam waist region; this data set is fitted to a model of the beam. The uncertainties, errors, and artifacts of the measurement procedure are analyzed by principal-component analysis. This study has made it possible to refine the measurement protocol and to identify, classify, and filter undesirable sources of noise. The iterative deconvolution algorithm stops when a well-defined threshold is reached. Spatial maps of mean values and uncertainties have been obtained for the beam irradiance distribution, the scanned spatial response data, and the resultant spatial responsivity of the infrared antenna. Signal-to-noise ratios have been defined and compared, and the beam irradiance distribution characterization has been identified as the statistically weakest part of the measurement procedure. © 2005 Optical Society of America

OCIS codes: 040.3060, 120.4800, 230.0250.

1. Introduction

Novel techniques and devices have been developed during the past decade to detect light. Among them, our research is focused on antenna-coupled detectors. They detect electromagnetic radiation in millimeter, infrared, and visible regions. The response of antenna-coupled detectors depends on the wavelength, the state of polarization, and the direction of the incident light.¹⁻⁴ The detector's size is of the same magnitude as the detected wavelength, typically of the order of a few micrometers, with spatial features on a nanometer scale. Currently, an active area of research is improvement of the sensitivity of these devices and their robustness to the presence of noise.

In a previous paper the general procedure for obtaining the spatial response of an infrared antenna when the device is illuminated with a focused laser

beam was described.² The laser beam profile is characterized by a knife-edge technique. This technique scans an aperture that has a straight line (typically made with a thin razor blade, a knife-edge) in such a way that the beam is progressively blocked (or unblocked if we move it in the opposite direction). The movement is perpendicular to the straight line that defines the edge. The signal behind the knife-edge is registered as a function of the position of the knife-edge. The signal corresponds to an integration of the irradiance of the beam. The limits of the integration change along the direction of the scan. These measured data are fitted with a beam irradiance model that takes into account diffraction and aberrations. The actual laser beam waist is scanned with the antenna in two dimensions. Thus this measured data set is taken as a convolution of the beam irradiance distribution at the beam waist and the true spatial response of the antenna. Finally, the true spatial response of the device is extracted from the measured spatial response through an iterative deconvolution technique.

Experimentally, we have two types of data: the knife-edge measurements used for characterizing the beam irradiance distribution and the maps of the signal detected by the infrared antenna when the beam waist plane is scanned. These two measurements are both affected by two types of fluctuation and uncertainty. On one hand, noise is present in the

J. M. López-Alonso and J. Alda (j.alda@fis.ucm.es) are with the School of Optics, University Complutense of Madrid, Avenida Arcos de Jalón, s/n, 28037, Madrid, Spain. B. Monacelli and G. Boreman are with the College of Optics and Photonics, Center for Research and Education in Optics and Lasers and Florida Photonics Center of Excellence, University of Central Florida, Orlando, Florida 32816-2700.

Received 15 November 2004; revised manuscript received 16 February 2005; accepted 20 February 2005.

0003-6935/05/214557-12\$15.00/0

© 2005 Optical Society of America

output of the infrared laser used to illuminate the antenna.⁵ In our case the fluctuations in the optical power emitted by the laser arise from the cooling mechanism used to stabilize its emission. On the other hand, there exists an uncertainty in the location of the device and the knife-edge that is due to positioning errors of the micropositioning system. For both types of data, these sources of noise influence the final output in a nonlinear manner.

Principal-component analysis (PCA) has proved its utility to reveal subtle noise structure in a wide variety of fields.^{6–9} It uses a covariance matrix to reinterpret original data as a collection of processes that are mutually uncorrelated and that can be identified with meaningful spatial–temporal structures, including noise identification. PCA also facilitates filtering of the original data to explicitly remove undesirable sources of noise. In this paper we describe the use of PCA to obtain an uncertainty map and to filter spurious signals for each data set of the measurement procedure. These uncertainty maps also define a signal-to-noise ratio (SNR) for both data sets. In comparing these SNRs we identify the statistically weakest point in the measurement procedure. Also, the PCA method makes it possible to define a threshold value that stops the iterative deconvolution algorithm at an appropriate point in the computation before it reaches nonphysical spatial responses.

In Section 2 of this paper we briefly introduce the PCA method, devoting specific attention to the capabilities of PCA method to identify, classify, and filter noise structures and artifacts in a data set. It is important to note that the results of the PCA method can be spatially displayed as images or maps. These maps will yield valuable insight for processing the measured data. In Section 3 we describe the sources of error and uncertainty in detail. The section is divided into three subsections, each devoted to an aspect of the measurement procedure: the beam irradiance distribution characterization, the measured spatial response of the infrared antenna at the beam waist, and the deconvolution algorithm used to extract the true spatial response of the detector from the measured response. PCA is introduced in each of these subsections to produce three important results, a mean value map, an uncertainty value map, and a SNR for each facet of the measurement. Finally, the main conclusions of the paper are summarized in Section 4.

2. Principal-Component Analysis

The general structure of a measurement is the estimation of a quantity g that is obtained from N variables, x_k . Typically, they are related by a function

$$g = f(x_1, \dots, x_k, \dots, x_N). \quad (1)$$

The uncertainty in variable x_k is characterized by its standard deviation. If quantity g can be described as in Eq. (1), we characterized the uncertainty of g by propagating the uncertainties of variables x_k in a well-known manner, following the so-called rule of

the propagation of variance.¹⁰ In the previous general framework it was assumed that we had a known functional relationship among the variables. But in some cases the relationship among variables is not functional and depends on complicated experimental procedures. Such is our case, for which the final results are obtained after fitting procedures and the application of an iterative deconvolution algorithm. To best estimate an uncertainty for our final result, we propose the use of a multivariate technique, PCA, in which not the original set of variables, x_1, \dots, x_N , but a linear combination of these variables is studied. These linear combinations produce a new set of variables, the principal components Y , that are mutually uncorrelated. The coefficients of these linear combinations are the eigenvectors of the covariance matrix, and the variances of the new variables Y are given by the eigenvalues of this matrix. The covariance matrix is defined by the following procedure: If M observations are taken of each k variable, these M instances can be arranged as $\bar{X}_k^T = (x_{1,k}, x_{2,k}, \dots, x_{M,k})$, where $x_{i,k}$ is the value of variable k at instance i . By use of this method the set of data is placed in an $M \times N$ matrix, X . The covariance of this set of data is defined by the following matrix: $S = (1/(M - 1))\bar{X}^T - \bar{X}$, where \bar{X} is a set of data that has zero mean. We obtained this modified set of data from the original set by subtracting its mean from each variable. A more detailed description of this procedure is given in Ref. 6. The relation between the original data and the principal components can be expressed as follows:

$$Y_\alpha = \sum_{k=1}^N e_\alpha(k)x_k, \quad (2)$$

where $e_\alpha(k)$ is element k of the α eigenvector. Moreover, the extraction of eigenvectors and principal components is arranged in decreasing order of the amount of variance contained in the given principal component. This means that the first principal components (those with the most variance) are the most important to describe the results. Furthermore, it is possible to define a parameter

$$\Omega_\alpha = \lambda_\alpha / \sum_{\alpha=1}^N \lambda_\alpha \quad (3)$$

that quantifies the percentage of the total variance explained by the α principal component, Y_α . Normally, a few principal components describe a large amount of the data variability. If such is the case, one can reconstruct data by using Eq. (3), taking into account only the relevant principal components^{6,11}:

$$x_k = \sum_{\alpha=1}^N e_\alpha(k)Y_\alpha. \quad (4)$$

Previously, a method to group principal components into relevant noise structures was developed^{6,7} based on a study of the uncertainties of λ_α . If two principal components have approximately the same variance,

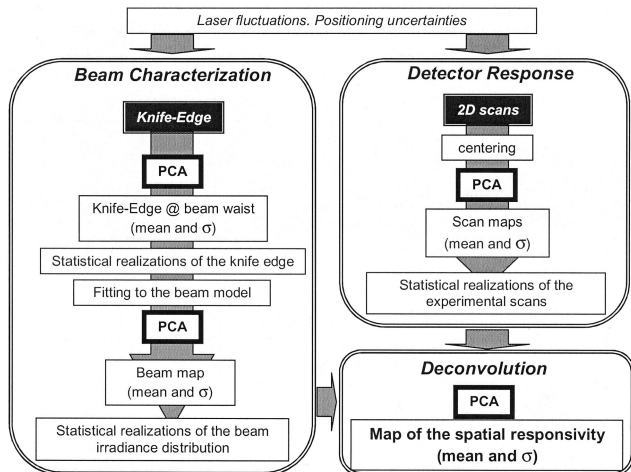


Fig. 1. Flowchart of the measurement procedure, highlighting the steps in which the PCA method is applied.

they explain the same amount of data variability. When this happens, the two principal components form a process, and we have to group them together in Eq. (4) to reconstruct the relevant data set.

The PCA method is well suited for application to the analysis of measurement uncertainties. During the measurement, some artifacts could be introduced into the data by the experimental apparatus. Some of these artifacts may have spatial-temporal structures that are clearly different from the signal or from random signal fluctuation. The PCA technique can be useful for classifying, quantifying, and filtering some of these structures. In this sense, it can be used as a tool for the characterization of measurement protocols.

3. Measurement Procedure

In this section we describe the measurement procedure. In infrared antennas the light of a CO₂ laser is focused onto the antenna through appropriate optics. The optical train contains collimation and focusing optics in addition to polarization state selection and temporal modulation subsystems. This procedure yields a linearly polarized and modulated laser beam focused on a small region. The antenna is then located inside this focal region, and a two-dimensional (2D) raster-scanned map of the detector response is measured. This measured map is the convolution of the beam shape with the true spatial response of the antenna. This response can be obtained by an iterative deconvolution algorithm.² The algorithm uses a modeled beam irradiance distribution that has been obtained from transverse knife-edge measurements.

Experimentally, the measurements are of two categories: signal and position. A signal is obtained either from the antenna, in the form of a voltage signal, or from an optical powermeter located immediately behind the knife-edge; the latter signal is proportional to the beam irradiance that is unobscured by the knife-edge. The position of the elements with respect to the laser beam is measured as a distance,

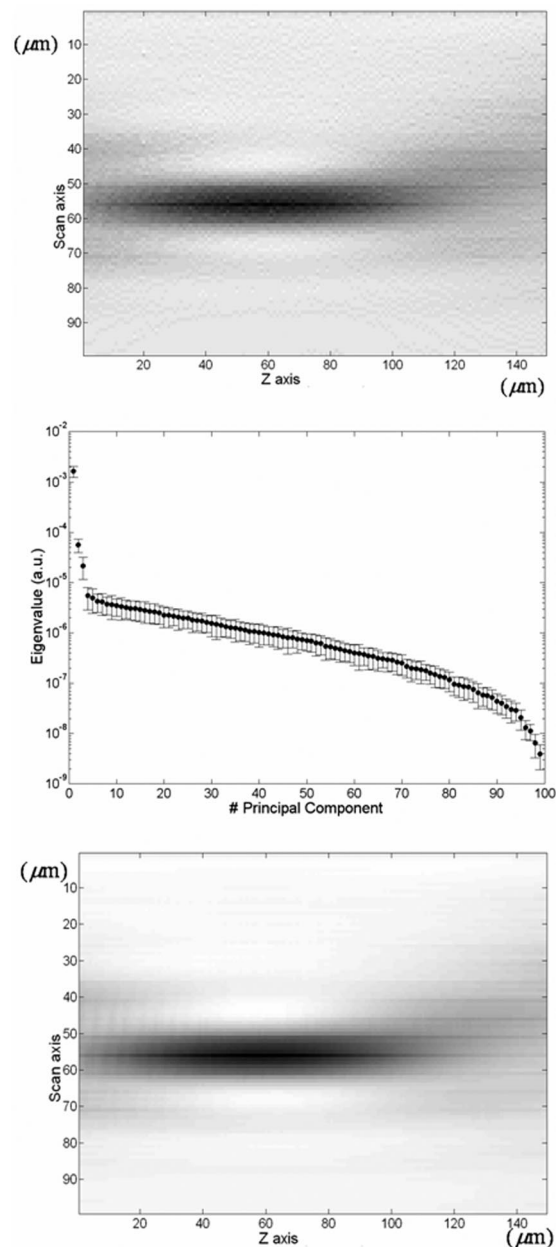


Fig. 2. Top, Knife scan original data after differentiation with respect to the scan coordinate (along the vertical axis); Horizontal axis, axis of beam propagation. Center, Eigenvalues and their uncertainties obtained after the PCA method is applied to the original data set. Bottom, filtered data set removal of random noise that corresponds to a principal-component group from Y_4 to Y_{100} .

usually in micrometers. For the signal category, the optical output of the laser is affected by fluctuations of its cooling system.⁵ The temporal period of these fluctuations is approximately 100 s. These fluctuations are transferred to the measured signal and affect the calculation of the location of the focus region. Moreover, there are random fluctuations of the laser mean output power superimposed upon the fluctuations that are due to the cooling system. For the position category the motorized stages used to produce the 2D scan maps are affected by uncertainties

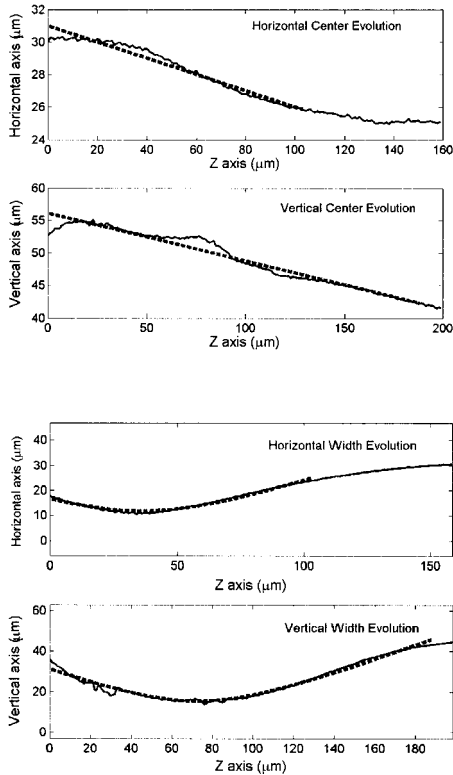


Fig. 3. Evolution of the first-order and second-order moments for the horizontal and vertical filtered knife-edge data. The plots of the first-order moment show a residual misalignment of the optical train. This misalignment is $\sim 2.8^\circ$ for the horizontal axis and $\sim 4.2^\circ$ for the vertical axis.

in position, both absolute and incremental. These uncertainties arise as a result of errors of stage motion such as backlash and wobble. These uncertainties further affect the evaluation of the beam irradiance and the fidelity of the 2D maps.

In the next subsections we describe how to process the data with respect to these error sources and the possibility of filtering some of their effects and artifacts. PCA is applied to filter undesirable contributions after their origins are identified. The original data are reconstructed by use of only meaningful principal components. The filtered data set is used to define a SNR for each type of measurement. A flowchart of the measurement procedure proposed here is shown in Fig. 1. The diagram shows how the experimental uncertainties are propagated in the characterization of the beam and to the scan of the detector response, finally to influence the map of the antenna's spatial responsivity. The PCA method makes possible the definition of the spatial map of the responsivity as well as the spatial map of the associated uncertainty.

A. Characterization of the Beam Irradiance

As stated above, the evaluation of the true spatial response of the antenna requires knowledge of the illuminating beam's irradiance distribution. To measure the antenna's spatial response, we locate the antenna where the irradiance is the largest. Our ex-

perimental setup contains an apertured and weakly aberrated Gaussian beam, so the beam irradiance is largest at the beam waist plane. The parametric characterization of the beam propagation establishes that the beam waist appears where the centered second-order moment of the beam irradiance reaches its minimum value (centering requires evaluation of the first-order moment of the irradiance distribution). However, this parametric characterization is not enough, because the spatial irradiance distribution is needed for the spatial characterization of the antenna response. Thus the characterization of the beam is made in two steps. The first step locates the position of the beam waist by monitoring the evolution of the knife-edge measurements and by calculating the first- and second-order moments. The second step fits the knife-edge scan data obtained in the beam waist region to the modeled beam.

Although the beam characterization can be made at any time during measurement, our experience with the measurement of infrared antennas indicates that the knife-edge measurements should be made before the measurement of the antenna spatial response. By performing the measurement in this manner, we may detect misalignments in the optical train and correct them before placing the detectors that we want to characterize. At this point we emphasize that knife-edge techniques intrinsically integrate the beam irradiance along the direction perpendicular to the scan. The experimental setup used in this task produces two knife-edge data sets by scanning the knife-edge along the two orthogonal directions perpendicular to the propagation axis. Then, if we assume that we have P points in each scan, we finally obtain $2P$ points in the measurement. It is clear from here that we will need some additional information to develop a 2D map of the irradiance distribution ($P \times P$ points). This additional information is obtained from the physical model of the beam irradiance distribution.

We locate the focal region by taking successive knife-edge measurements over different ranges of axial coordinate Z (Z is along the direction of beam propagation). By varying the step in Z (from coarse to fine, which is limited in our experimental setup to $1 \mu\text{m}$ resolution) while contracting the range of Z as the resolution is increased, we may finally locate the focal region and adapt the scanning to the finest step. To characterize this region of exact focus, we perform two orthogonal transverse scans in that focal region. Then we take the spatial derivative of each transverse scan profile with respect to the scanning coordinate. The differentiated profiles are used to evaluate the first- and second-order moments of the laser beam as a function of the axial coordinate. These derivatives contain the integration along the coordinate orthogonal to the scanning direction. This fact does not affect to the validity of the evaluated second-order moments. Beam waist position is located by a parabolic fit of the second-order moment. The waist location is also obtained from this fit. The

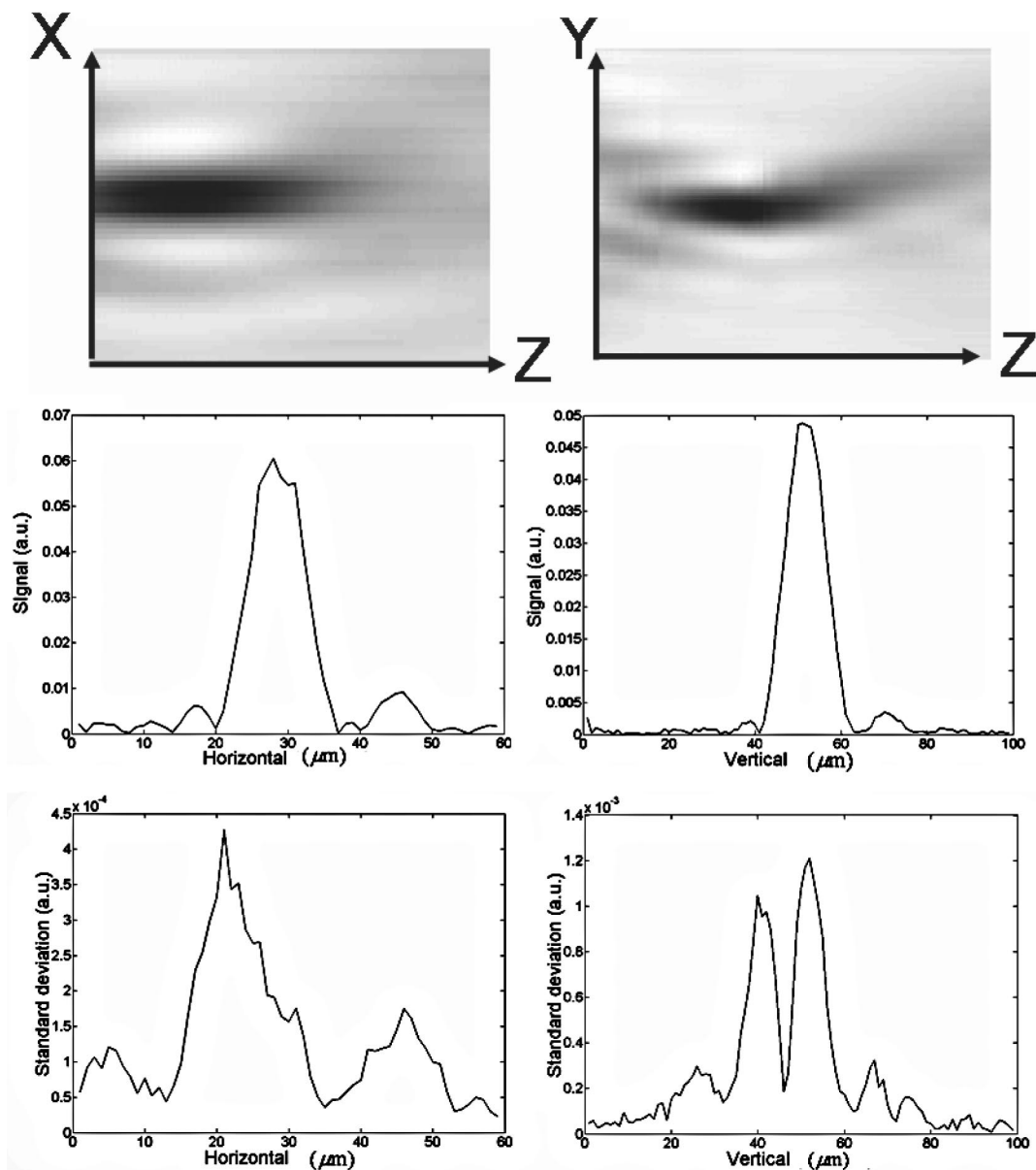


Fig. 4. Top, filtered knife-edge data for the horizontal (left) and vertical (right) directions. After the beam waist location and depth are defined it is possible to obtain the averaged beam profiles (center) and their uncertainties (bottom).

beam waist constitutes the focal region where the antenna is located during its characterization.

The main limitation of this procedure is the sensitivity of the second-order moment estimation to the noise level of the data set. The top portion of Fig. 2 shows the derivative of the original knife-edge scans. The noise is superimposed upon this image. This noise comes primarily from the slowly varying power fluctuations of the laser. To reduce these fluctuations we include a reference detector that measures the optical output of the laser at the same instant as the knife-edge data are taken. Then the knife-edge scan data are normalized with respect to this reference. This procedure takes into account the variation in the mean signal value but not other sources of noise fluctuation.

The experimental data are processed by PCA. Each knife-edge scan data set is taken as a random variable. The center of Fig. 2 represents the eigenvalues obtained from the PCA method applied to the top map of Fig. 2. Four processes can be defined: The last process comprises the majority of principal components (from Y_4 to Y_{100}) and can be identified with a random noise. It explains 6% of the total data variance. When the data set is reconstructed without this process, the bottom map of Fig. 2 is obtained. The spatial beam evolution is maintained, and the random noise is removed. With this filtering procedure it is possible to locate the center of beam waist with better accuracy. We then located the beam waist by fitting the second-order moment evolution to a parabolic function (see Fig. 3). The location of the mini-

mum of this parabolic fit is the focus. It is possible to obtain an uncertainty for this focal position that is due to the uncertainty of the fitting. The previous procedure is applied to laser knife-scans in two transverse directions (horizontal and vertical), orthogonal to the beam propagation direction. After that, the integrated beam shape in each direction is calculated at this focus position by use of filtered data. The uncertainty in the best focus position defines a region, instead of a point, where the beam waist is located. Then an uncertainty in the integrated beam irradiance distribution is calculated as the standard deviation of the integrated beam profiles within the focal region. Figure 4 shows the filtered knife-edge data at the top, the beam irradiance profiles in the center, and the uncertainty of this irradiance at the bottom.

Previously the laser beam profile was modeled as the irradiance distribution that results from the convolution of a Gaussian beam with an aberrated and diffracted field distribution.² Owing to the characteristics of the optical train, it is possible to ensure that the main contribution to the wave-front aberration comes from coma. Actually, the presence of coma ($\sim 0.1 \lambda$) in the wave-front aberration function) can be detected when one is analyzing some measured scans made with antenna-coupled detectors. The typical comatic shape is observed in those scans. In our optical train, coma appears because of residual misalignment. This misalignment is evaluated from the evolution of the first-order moment of the differentiated knife-edge measurements (shown in Fig. 3). The analytical form of the beam model is

$$E(x, y) = \exp\left(-\frac{x^2 + y^2}{\omega_0^2}\right) \left(\frac{2J_1(v)}{v} - \alpha \cos \phi \frac{2J_4(v)}{v} - \alpha^2 \frac{1}{2v} \times \left\{ \frac{J_1(v)}{4} - \frac{J_3(v)}{20} + \frac{J_5(v)}{4} - \frac{9J_7(v)}{20} - \cos 2\phi \left[\frac{2J_3(v)}{5} + \frac{3J_7(v)}{5} \right] \right\} \right), \quad (5)$$

where

$$v = \frac{2\pi}{\lambda} \frac{a}{z} (x^2 + y^2)^{1/2}, \quad (6)$$

λ is the laser wavelength, ω_0 is the Gaussian beam width, a is the size of the aperture, z is the distance of observation (here it coincides with the focal length of the illumination system), α is the amount of aberration expressed as a fraction of the wavelength, and ϕ is the angle of orientation of the coma aberration. This model was used successfully previously for the deconvolution of the spatial response of several types of infrared antenna.^{2,3,12}

Once the model is set, we obtain the beam profile used in the deconvolution by fitting the experimental data obtained from the knife-edge measure-

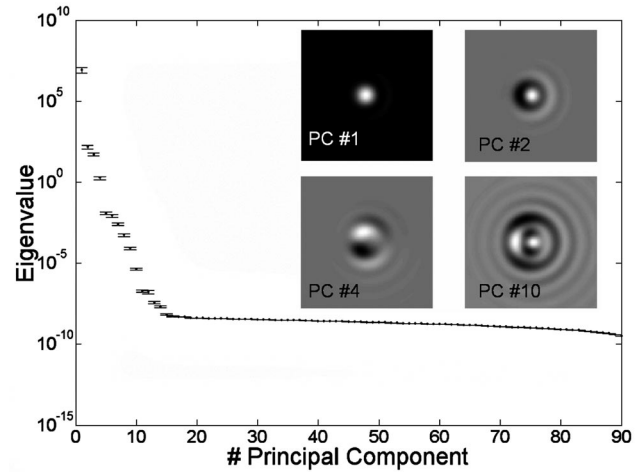


Fig. 5. PCA applied to the modeled beam irradiance distribution. The original distributions are generated by fitting of the modeled beam with the data obtained for the beam waist region after a collection of knife-edge profiles is generated that takes into account the uncertainties of the data. The general spatial structure of the beam is explained by Y_1 – Y_{14} . The rest of the principal components (PCs) are related to numerical noise introduced by the fitting algorithm and therefore can be filtered out.

ments to simulated knife-edge data based on the modeled beam. We make the fit by minimizing a merit function that is defined as the mean-square difference between the experimental and the simulated data. This procedure was studied by the PCA method as follows: We have shown that the knife-edge measurement produces two mean integrated profiles, one for each transverse direction, along with two profiles of uncertainty (as shown in Fig. 4, bottom). By using the means and uncertainties in the profiles we generated a collection of 100_{X-Y} pairs of knife-edge profiles. We obtained the knife-edge profiles by assuming at each point a Gaussian probability distribution with a mean value given by the mean value at this point, and a standard deviation given by the uncertainty at that same point. Each pair of knife-edge scans was independently fitted to a laser beam irradiance based on the beam model of Eq. (6). Finally, PCA was applied to the modeled set of beam irradiance distributions. Our objective was to identify the spatial structures arising from the uncertainty of this fit. These structures have an important role during the deconvolution required for recovering the spatial response of the antenna. The eigenvalues of the principal components appear to be grouped into two subsets (see Fig. 5). The largest subset comprises principal components from Y_{15} to Y_{100} , and it describes the numerical uncertainties introduced by the fitting algorithm. The other subset of principal components, Y_1 – Y_{14} , is responsible for the spatial structure of the beam irradiance. The first component comprises 99.99% of the total beam-shape variance. This shows the high sensitivity of the PCA method to subtle differences between structures.

According to the process described by Eq. (4), the beam shape is filtered to suppress the numerical fit-

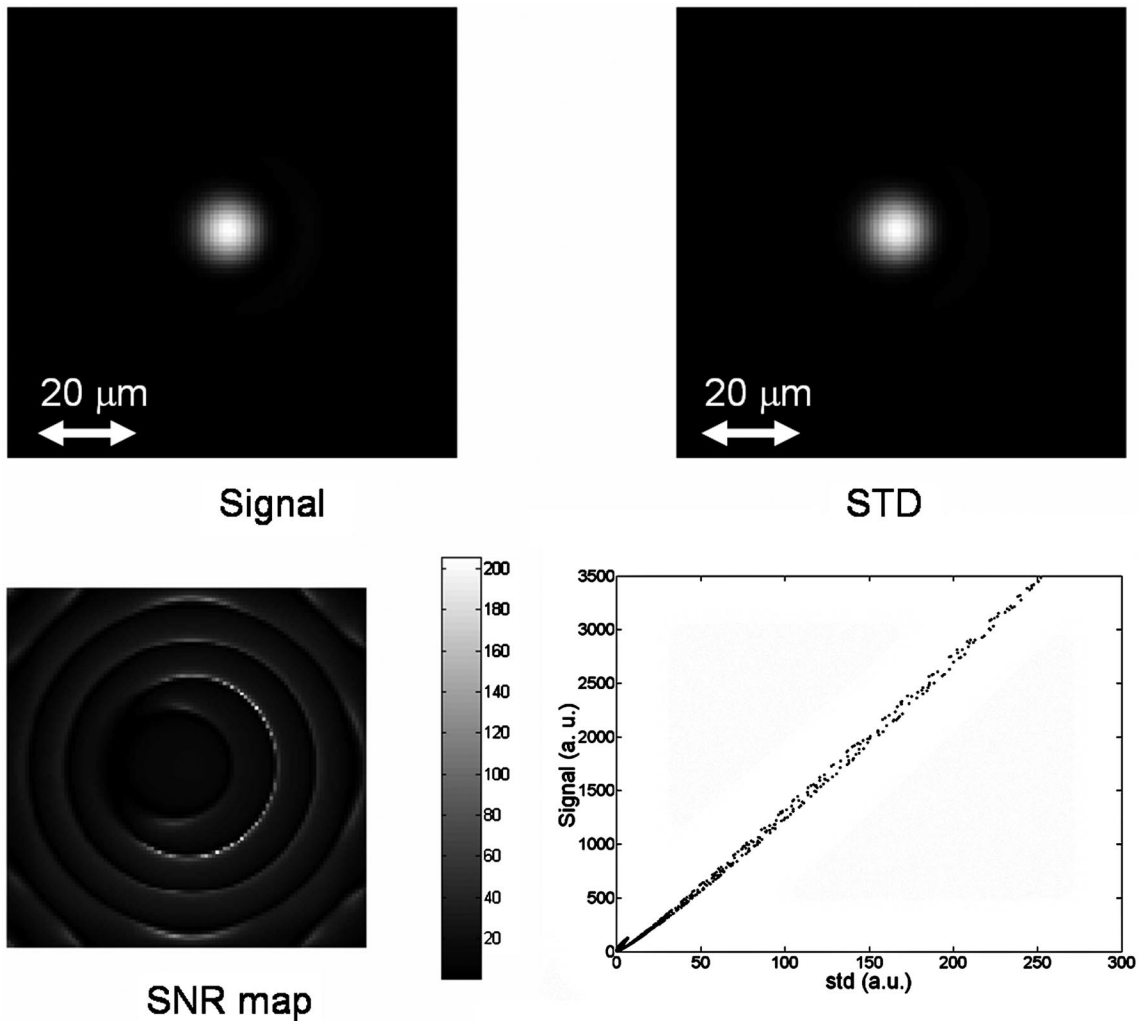


Fig. 6. Mean irradiance distribution (left, top) and its standard deviation (STD; right, top). The SNR map is obtained after division of the previous two maps (left, bottom). Representing the SNR for all the points yields the figure at bottom right. Fitting these points to a linear function yields a global SNR_{beam} .

ting noise; only principal components Y_1 to Y_{14} are taken into account. The mean value of the filtered data set is a 2D beam distribution, which we define as the signal. The standard deviation within the filtered data at each spatial location can be seen as a 2D map of the uncertainty (or noise) in the determination of the beam irradiance. From these two spatial distributions one can obtain a SNR map by dividing the signal and the standard deviation at each location. Plotting the mean value versus the standard deviation allows us to consider the slope a global SNR for the laser beam. In this case $\text{SNR}_{\text{beam}} = 13.27 \pm 0.02$. The uncertainty in this value is due to the linear fit of this slope. All maps and fit data are represented in Fig. 6. The value of the SNR can also be used to define the relative noise of this part of the measurement process. This relative noise is given as

$$\varepsilon = 1/\text{SNR}. \quad (7)$$

Then, applying this definition, we obtain $\varepsilon_{\text{beam}} = 0.07536 \pm 0.00011$.

B. Infrared Antenna Measurement

In this analysis we measure dipole antenna-coupled infrared detectors. The length of the dipole under test is $5 \mu\text{m}$. The antenna is located within the beam waist region. We find this location by moving the detector in front of the beam to maximize the value of the detected signal. We assume that the maximum signal is obtained when the center of the beam waist coincides with the center of the infrared antenna. After that, several 2D scans are taken, and the PCA method is applied. In the case considered here, we have nine 2D maps. Each consists of a matrix of 85×85 points with a step (resolution) of $1 \mu\text{m}$. These points are successively obtained in a raster-scan fashion.

Because of uncertainties in the reset position of the motorized stages, the responsivity maps are not centered at the same position for different maps. Moreover, the fluctuations of laser signal are going to affect the response signal level of each map. To quantify these effects, we again apply PCA to two 2D scan data sets. The first set contains the original

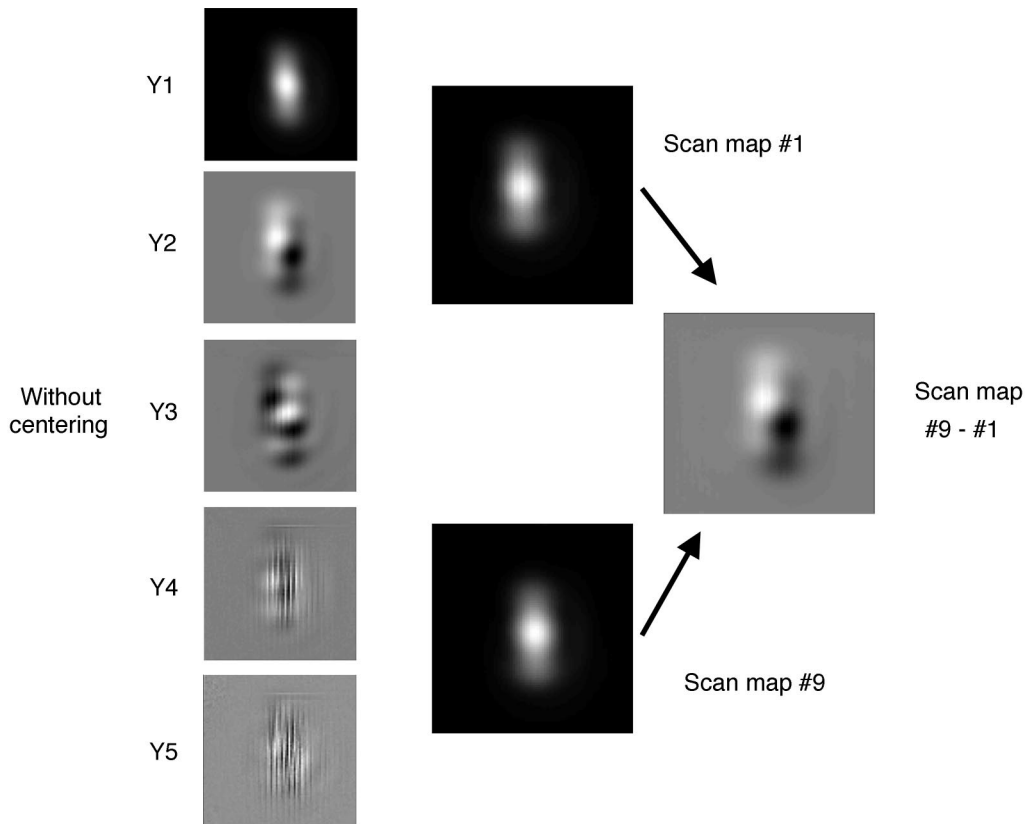


Fig. 7. Images that correspond to principal components Y_1 , Y_2 , Y_3 , Y_4 , and Y_5 obtained from a collection of nine experimental 2D scan maps (left) column from upper to lower). These scan sets are not centered. Center, original 2D scan maps #1 and #9. The difference between these maps reveals the effect of decentering the data. This subtraction image resembles the Y_2 map, again illustrating the filtering power of PCA.

2D scan data set, and the second set is obtained after the data are centered to coincide with the first data set. The second data set is obtained and repositioned after the first-order moments of both maps along each direction are calculated because the first-order moment of the detected signal map defines its center. Then the original maps are cropped to produce images of a reduced size (71×71 points) and coinciding centers.

In the center of Fig. 7 we have plotted original 2D scan maps #1 and #9. The difference between these two maps is the largest of all the mutual differences between two maps. It is possible to see how the position of the center of the original scans changes from one image to the other. The right-hand side of Fig. 7 contains the subtraction of the original scans, scan map #1 minus scan map #9. The result of this subtraction is clearly similar to the second principal component, Y_2 . The top of Fig. 8 shows the eigenvalues of PCA decomposition with and without centering of the images. The eigenvalue analysis shows more components for the decentered than for the centered case. Therefore we may conclude that these additional components are related to decentering artifacts, as we can also prove by analyzing the principal components obtained for the original data. The left-hand side of Fig. 7 shows principal components Y_1 , Y_2 , Y_3 , Y_4 , and Y_5 obtained from one of the original

2D scans. Furthermore, when the PCA method is applied to the centered data sets, only two types of principal component appear (see Fig. 9). At the bottom of Fig. 8 we have plotted the evolution of the location of the center of the data for the nine experimental scans. The center positions of the maps change as a result of uncertainties in resetting the motorized stages after each scan. This figure shows how the vertical direction (Y direction) is more affected by this error because the vertical stage is supporting the weight of the antenna circuit, and this introduces more uncertainty when the stage returns to the fiducial position.

The first principal component of the centered data set, $Y_{1, \text{cent}}$, has the same weight in every centered scan. Also, it is equal to the first principal component obtained from the original (noncentered) data. The rest of the principal components resemble the structure of component Y_4 and consecutive components obtained from the original data (Fig. 7, left). The structure of this last group of principal components is quite interesting and reveals other sources of spatial-temporal noise. They have a structure of lines that correspond to different levels on the signal. This structure is caused by fluctuations of laser optical power. This conclusion is supported in the temporal dependence of the data. The map obtained here is collected after a 2D raster scan. The time from one

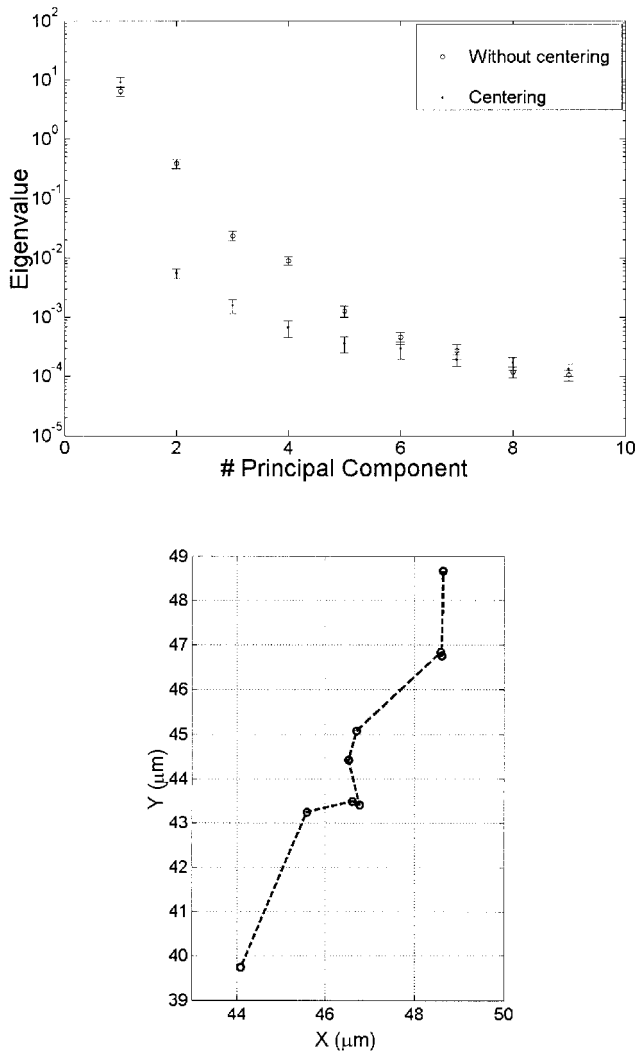


Fig. 8. Top, eigenvalues for decentered and centered data. Bottom, evolution of the location of the data center in the XY plane.

datum to the next is ~ 1 s. When one is rearranging the map into a temporal series, it is possible to perceive a temporal variation that has a period of ~ 100 s. This period coincides with the laser cooling system's time cycle. Despite its mixed spatial-temporal structure, one can remove this signal from the data by filtering with the PCA method.

From the previous analysis we may reconstruct the original data with only the first principal component obtained from the PCA method after centering the data, $Y_{1, \text{cent}}$. The new set of data consists of nine images. The mean value of this data set is the 2D scan map that we define as the signal. The standard deviation for each pixel can be taken as a 2D map of the uncertainty of the signal. From these two maps we can obtain another SNR map by dividing the signal and the standard deviation at each location, as shown in Fig. 10. The value of $\text{SNR}_{\text{scans}}$ is 54.13 ± 0.08 . On applying the definition for the relative noise, [Eq. (7)] we obtain $\varepsilon_{\text{scans}} = 0.01847 \pm 0.00003$. This procedure rejects the influence of spurious laser fluctuations and

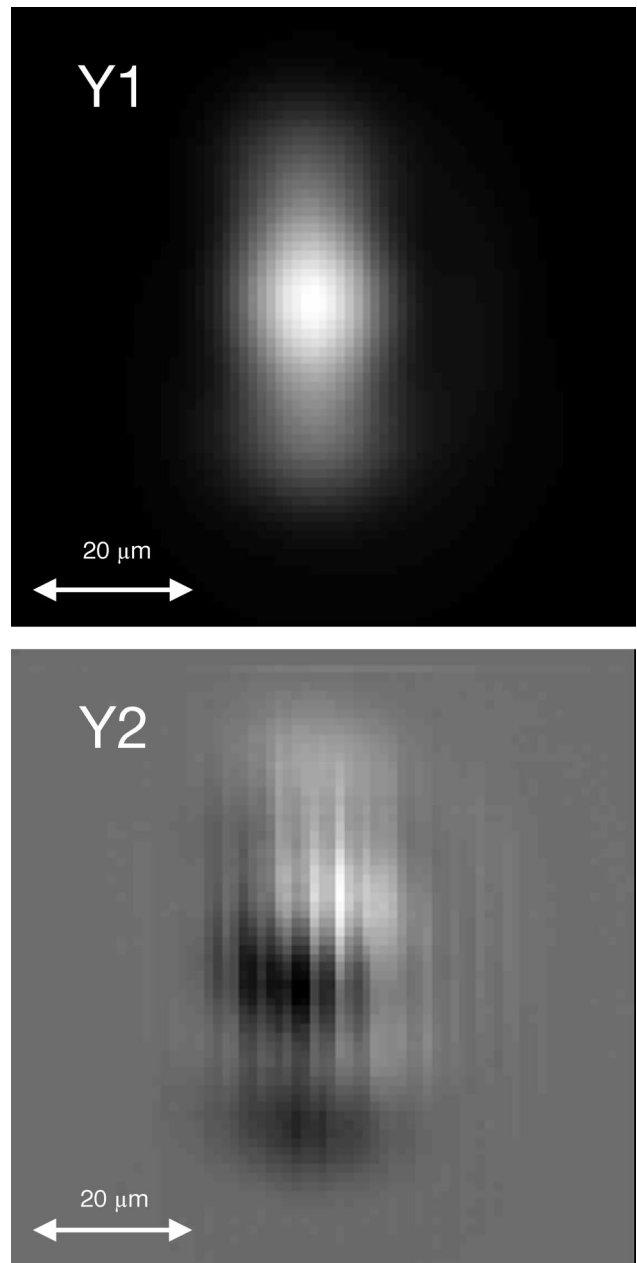


Fig. 9. The PCA method applied to the centered data provides a first principal component Y_1 (top), which is the same as that obtained from the original data, and a second principal component Y_2 , which contains information about the effect of the cooling system's influence on the laser output.

takes into account the uncertainties introduced by the centering procedure. The value of $\text{SNR}_{\text{scans}}$ is larger than that of SNR_{bcam} .

C. Deconvolution Procedure

At this point we have a 2D map representing the experimental response of the infrared antenna illuminated by the laser beam (and its associated 2D map of uncertainties) and another 2D map that contains the modeled laser beam irradiance distribution (and its map of uncertainties). The 2D map of the experimental response is taken as the convolution of the beam irra-

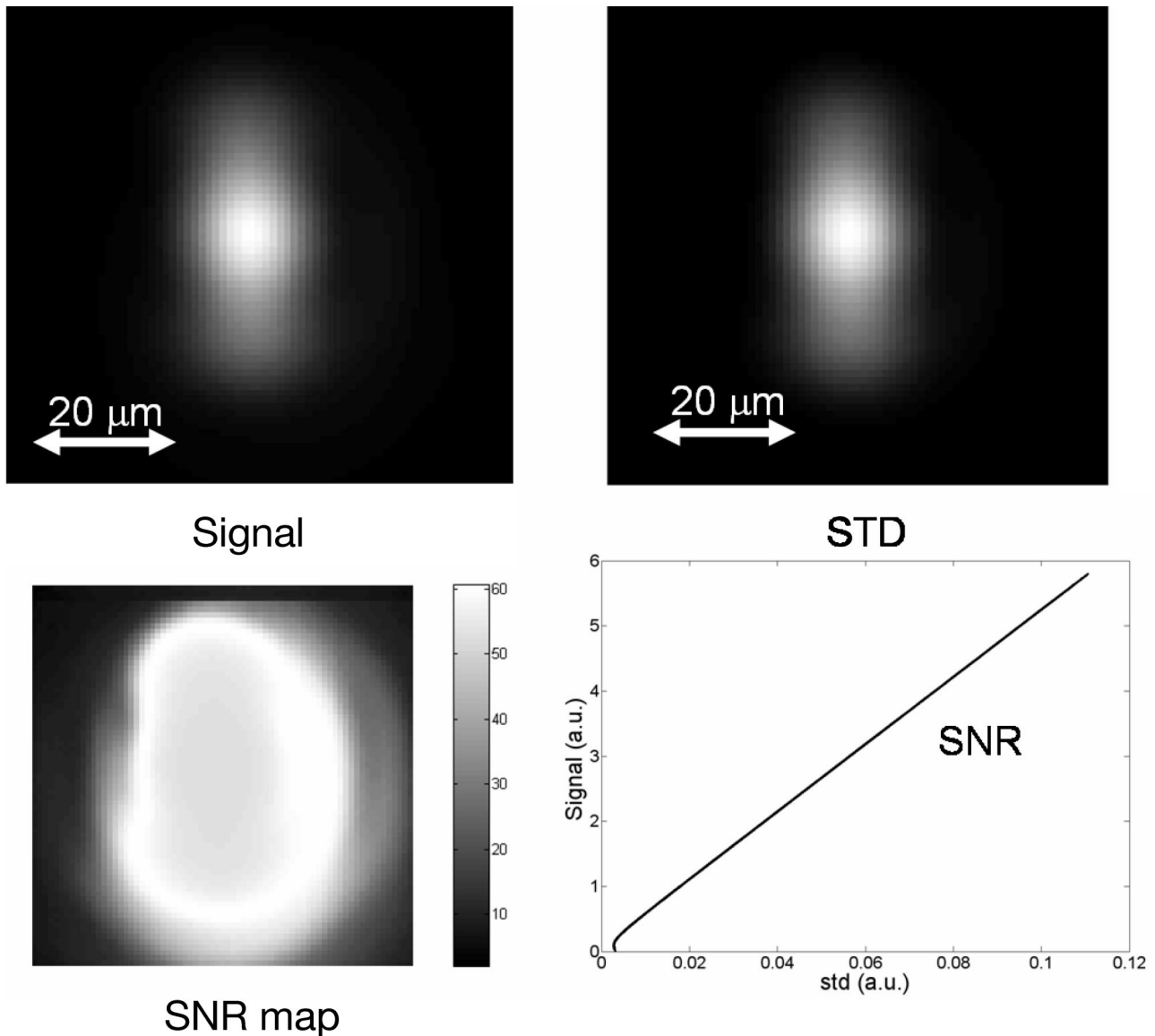


Fig. 10. Application of the PCA method to the 2D maps permits definition of an averaged map (top left) and a map of its standard deviation (STD; top right). From these two images it is possible to obtain the map of the SNR (bottom left) and a mean value of this parameter SNR_{scan} after the SNR data are fitted with a linear function.

diance distribution with the actual spatial responsivity of the antenna-coupled detector. The final goal in the characterization of these detectors is the evaluation of their actual spatial responsivity map, which we obtain by deconvolving the beam irradiance distribution from the experimental signal map. A Lucy–Richardson algorithm is used for this purpose.^{13,14}

We use the following procedure: First we generate different pairs of beam shape and 2D scan map responses, using their mean values and uncertainties. We accomplish this by adding to each pixel of the mean value map a random number according to a Gaussian distribution with a standard deviation given as the uncertainty of that pixel. Then the beam irradiance distribution is deconvolved from the 2D scan map response. After each step, a merit function is calculated as the mean-square error of the differ-

ence between the convolution of the beam irradiance distribution with the calculated spatial response and the original measured 2D scan map. It is possible to calculate a threshold of this merit function because we know the uncertainty of each pixel of the 2D scan map response. Therefore it is possible to calculate a mean-square error. When the mean-square error obtained by the deconvolution procedure is lower than the threshold value, the iterative algorithm stops and the actual spatial responsivity of the infrared antenna is taken as the result of the algorithm.

After R iterations of the previous procedure we obtain a collection of R antenna responsivity maps. Again, it is possible to calculate a mean responsivity map and its uncertainty map by taking the mean value and the standard deviation of each pixel (see Fig. 11). The SNR is calculated according to the pro-

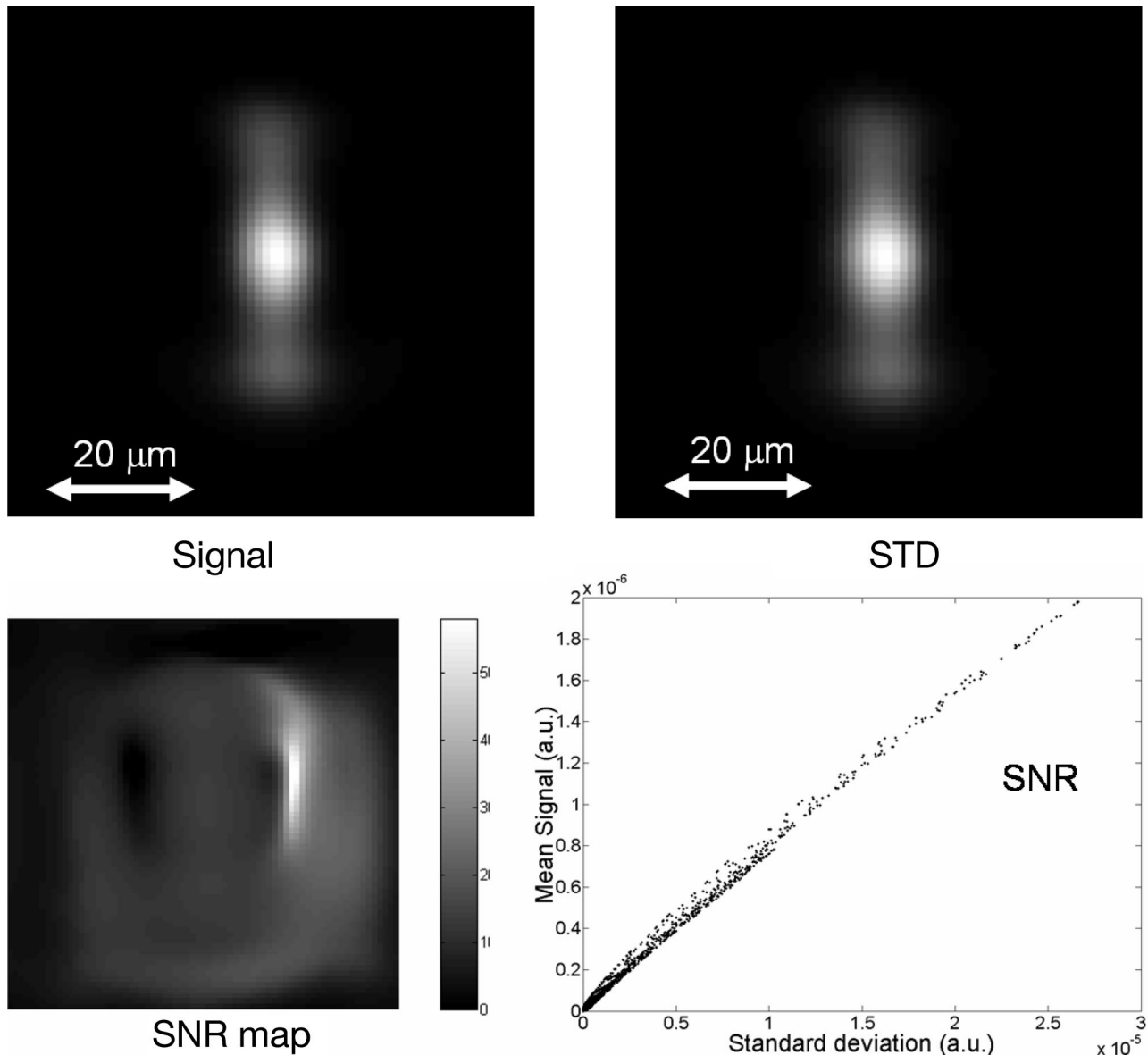


Fig. 11. Antenna's spatial response (top left) and its uncertainties [standard deviation (STD), top right]. These maps are obtained after deconvolution of the signals and application of the PCA method to the deconvolved results. Bottom left, spatial structure and value of the SNR. Linear fitting of the individual values of the SNR provides a global $\text{SNR}_{\text{respons}}$ value.

cedure explained above. The result is $\text{SNR}_{\text{respons}} = 12.73 \pm 0.02$. The corresponding value for the relative noise is $\varepsilon_{\text{respons}} = 0.07855 \pm 0.00012$. The spatial map of $\text{SNR}_{\text{respons}}$ is shown in Fig. 11.

We may check whether the beam irradiance distribution calculation and the measured response of the device are statistically independent. We can do this by evaluating $\varepsilon_{\text{bcam}}^2 + \varepsilon_{\text{scans}}^2 = (602 \pm 7) \times 10^{-5}$. This result is quite close to, but less than, $\varepsilon_{\text{respons}}^2 = (617 \pm 2) \times 10^{-5}$. The uncertainties' intervals almost overlap. We conclude that both inputs are approximately statistically independent.

4. Conclusions

In this paper we have presented a detailed procedure with which to calculate the spatial response of an

infrared antenna and the uncertainties in its evaluation. We have taken into account the principal sources of uncertainties in the measurement procedure, using the PCA method. Our approach has detected subtle signal fluctuations and artifacts: influence of the laser cooling system on the laser optical power, decentering artifacts of the detector positioning stages, and numerical fluctuations that arise from the fitting algorithms. PCA has also been used to filter the original data sets, permitting calculation of spatial maps of the signal mean value and uncertainties.

Two types of data have been analyzed separately. On one hand, we have taken knife-edge measurements and the fit of these data with a beam irradiance distribution model. On the other hand, we have

processed the data measured from the scanned response of the antenna-coupled detectors. We utilized both types of data to obtain the actual spatial response of the antenna by means of a Lucy–Richardson deconvolution method. The uncertainties in the measured scanned data define a mean-square error threshold. Therefore, after defining a merit function of the deconvolution algorithm, we used this threshold to stop the iterative deconvolution algorithm automatically. Employing this procedure, we obtained a collection of antenna spatial response maps and a mean response map with associated spatial uncertainties. SNR maps have also been defined for each portion of the measurement procedure. From each of these maps we obtained a global SNR value. The values obtained here are $\text{SNR}_{\text{bcam}} = 13.27 \pm 0.02$, and $\text{SNR}_{\text{scans}} = 54.13 \pm 0.08$. These two elements serve as inputs for the deconvolution algorithm that calculates the final spatial responsivity map of the detector. The final SNR for the spatial responsivity is $\text{SNR}_{\text{respons}} = 12.73 \pm 0.02$. On comparing these SNR values we may conclude that the input from the scanned detector response is of better quality than the input from the beam irradiance distribution. At the same time, by evaluating the relative noise we conclude that these two measurements can be taken as almost statistically independent because

$$\varepsilon_{\text{bcam}}^2 + \varepsilon_{\text{scans}}^2 < \varepsilon_{\text{respons}}^2.$$

The beam-shape characterization is thereby identified as the most prominent source of uncertainty in the whole measurement procedure. It limits the maximum achievable $\text{SNR}_{\text{respons}}$. To understand this we need to look back to the source of the data. Assuming that we need an irradiance distribution of $P \times P$ points to input into the deconvolution algorithm, the available amount of knife-edge data comes from two series of P points (assuming for simplicity that the step in the knife-edge and the step in the antenna scan measurements are equal and that the number of points along the transverse directions are identical). Therefore, the beam model has to satisfy the lack of information between the $2P$ measured points of the knife-edge scan and the P^2 points of the 2D scanned

antenna response maps. It is evident that a refinement either of the beam model or of the knife-edge measurement strategy would improve the SNR of the final spatial responsivity output.

References

1. C. Fumeaux, G. Boreman, W. Herrmann, F. Kneubühl, and H. Rothuizen, "Spatial impulse response of lithographic infrared antennas," *Appl. Opt.* **38**, 37–46 (1999).
2. J. Alda, C. Fumeaux, I. Codreanu, J. Schaefer, and G. Boreman, "A deconvolution method for two-dimensional spatial-response mapping of lithographic infrared antennas," *Appl. Opt.* **38**, 3993–4000 (1999).
3. I. Codreanu and G. D. Boreman, "Integration of microbolometers with infrared microstrip antennas," *Infrared Phys. Technol.* **43**, 335–344 (2002).
4. F. J. Gonzalez, M. A. Gritz, C. Fumeaux, and G. D. Boreman, "Two dimensional array of antenna-coupled microbolometers," *Int. J. Infrared Millim. Waves* **23**, 785–797 (2002).
5. J. M. López-Alonso, B. Monacelli, and G. D. Boreman, "Infrared laser beam temporal fluctuations: characterization and filtering," *Opt. Eng.* (to be published).
6. J. M. López-Alonso, J. Alda, and E. Bemabéu, "Principal components characterization of noise for infrared images," *Appl. Opt.* **41**, 320–331 (2002).
7. J. M. López-Alonso and J. Alda, "Characterization of artifacts in fully-digital-image-acquisition systems. Application to web cameras," *Opt. Eng.* **43**, 257–265 (2004).
8. J. M. López-Alonso and J. Alda, "Correlation in finance: a statistical approach," in *Noise in Complex Systems and Stochastic Dynamics II*, Z. Gingl, ed., *Proc. SPIE* **5471**, 311–321 (2004).
9. J. M. López-Alonso and J. Alda "Characterization of dynamic sea scenarios with infrared imagers" *Infrared Phys. Technol.* **46**, 355–363 (2005).
10. International Organization for Standardization, *Guide to the Expression of Uncertainty in Measurements* (International Organization for Standardization, 1993).
11. D. F. Morrison, *Multivariate Statistical Methods*, 3rd ed. (McGraw-Hill, 1990), Chap. 8.
12. C. Fumeaux, J. Alda, and G. D. Boreman, "Lithographic antennas at visible frequencies," *Opt. Lett.* **24**, 1629–1631, (1999).
13. W. H. Richardson, "Bayesian-based iterative method of image restoration," *J. Opt. Soc. Am.* **62**, 55–59 (1972).
14. L. B. Lucy, "An iterative technique for the rectification of observed distributions," *Astron. J.* **79**, 745–754 (1974).